Autonomous Pick-And-Place of a Novel Robotic Surgery Imaging Rail Using the dVRK Platform*

C. D'Ettorre, A. Stilli, G. Dwyer, M. Tran, D. Stoyanov

***Abstract*— During Robotic-Assisted Partial Nephrectomy (RAPN) part cancer cells encapsulated by a tumor in the kidney are excised. Ultrasound (US) imagining is used as an intra-operative technique to identify and outline the target tumor. During the surgical procedure, executed with the da Vinci Surgical System (Sunnyvale, CA), the US probe is usually "dropped-in" through an auxiliary access port, it is then grasped by the robotic tools and swiped on the surface of the kidney because US requires contact to deliver a signal. Slippages are really common during US scanning, causing continuous repositioning of the probe on the target organ surface and when the tumor is in difficult to reach regions management of the probe is cumbersome and awkward.**

This paper introduces a hardware setup and software architecture, customized for a novel imaging support system, designed in order to automate part of this surgical procedure to make workflow easier. The new system takes a very different approach to imaging probe navigation for drop-in US by using a vacuum sucker rail attached on the kidney surface to guide the probe's trajectory and slide. With this paper, we aim to automatically grasp the sucker rail and adequately locate it on the kidney surface so that the surgeon is then allowed to start manually manipulating the US probe along it. The system's workflow is based on a calibrated environment with a new comparison of real kidney surface registration and a controlled scheme applied on a pre-planned trajectory. We use a preliminary clinical study with four surgeons to evaluate the potential performance and workflow for using this new system design.

I. Introduction

Recent developments in robot-assisted laparoscopic interventions allow for dexterous, hand tremor filtered, enhanced surgical ergonomics which all facilitate highly precise movements within the internal anatomy without direct access. This has led to a growth in robotic surgery with over one million surgical procedures performed using the da Vinci Surgical System (Sunnyvale, CA) [1], as a potentially enhanced alternative to traditional laparoscopic surgery. Despite the increased uptake of surgical robotics, automation through the robotic platform is not currently available in clinical practice and has complex regulatory considerations. Nevertheless combining current technology with different control schemes could overcome many tedious surgical tasks by performing them automatically. This could significantly reduce the surgeon workload and enhance the user experience or even potentially minimize the likelihood of human error.

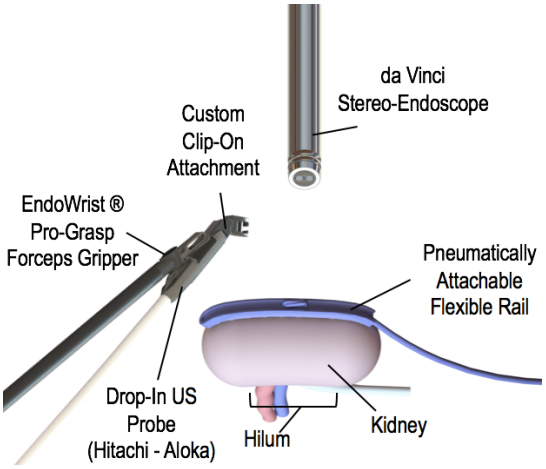

Fig. 1: model representation of the new design system. The sucker rail is located on the kidney surface and the model of US-probe is equipped with an adaptor. This allows the surgeon to properly grasp the probe with the Pro-Grasp tool and slide the probe in the rail. This revolutionized the acquisition protocol in case of intra-operative ultrasound acquisitions.

A. Problem Statment

Robotic-Assisted Partial Nephrectomy (RAPN) consists in the partial removal of kidney tissue in case of a tumor. After prostatectomy, RAPN is the second most common robotic-assisted surgical procedure worldwide [2], due to high prevalence (63,390 new cases/year) and mortality (13,860 death/year) of kidney cancer. Removal of the kidney tumor, leaving the rest of the kidney intact, has been shown to maximize the patients post-operative kidney function [3]. RAPN can be used in place of total nephrectomy or open surgery in some complex renal tumor cases as argued in [4]. Kaul et all [5] carefully described the entire surgical procedure.

Generally, the intra-operative identification of the tumor can be achieved through different techniques, including pre-operative Computer Tomography (CT), Magnetic Resonance (MR), and intra-operative ultrasound (US). Because pre- and intra-operative imaging can differ, increasingly intra-operative US is used to assist the localisation and targeting of pathological tissue during surgery when tissue differentiation is possible in the US image. Intra-operative characterisation

*This research is supported by the Wellcome / EPSRC Centre for Interventional and Surgical Sciences (WEISS) and from the EPSRC Impact Acceleration Accounts (IAA) 201720: Discovery-to-use funding.

C. D'Ettorre, A. Stilli, G. Dwyer and D. Stoyanov are with the Centre for Medical Image Computing (CMIC) and the Department of Computer Science, Wellcome/ EPSRC Centre for Interventioal and Surgical Sciences (WEISS), University College London, London W1W 7EJ, UK {c.d'ettorre@ucl.ac.uk}

M. Tran is with the Department of Nanotechnology, Division of Surgery and Interventional Science, University College of London, Royal Free Hospital, London NW3 2QG, UK

and delineation of tissue facilitates the surgeon to define optimal dissection planes and can potentially avoid injuries to critical anatomical structures as well as assist the preservation of healthy tissues.

Manual control of the US probe during surface scanning can significantly increase the cognitive load of surgeons, due to the need to maintain optimal scanning orientation and consistent contact with the tissue while simultaneously interpreting US image. Sometimes the localization of tumor might be inaccurate due to particular position hard to reach by the probe, which requires continuous repositioning because of slippage from the target organ surface. Recently it has been shown that the automation of repetitive surgical tasks or tasks that require high precision can be beneficial in improving accuracy and reducing the surgeon's cognitive load.

B. Related Work

Image-guidance within the da Vinci's console has been demonstrated for RAPN either with displaying 2D CT slices of a phantom to guide resection based on a point-based registration [6]. Kidney deformation effects have been explored due to fluid loss during incision of a real kidney after registering it to medical images [7]. Benincasa et al. [8] performed a study on surface point acquisition, defining which points acquired to obtain an accurate surface registration. More recently, a comparison between three different surface acquisition intra-operative methods has been done in [9].

A new design for "pick-up" US transducer was proposed by Schneider at al [10]. This system is compatible with the da Vinci's tool and allows to map the vasculature surfaces within the kidney for registration. Instead, in [11] regarding the US-scanning phase an auxiliary robotic arm holding an ultrasound probe is used to follow the motion of a teleoperated arm such that guidance can be provided to the surgeon during tumor resection. Vienne et al. [12] proposed a 6-DoF US visual servoing approach to control an US embedded in a robotic system.

A new framework for automatic tumor dissection for planar tissue surface has been designed in [13] using intraoperative US. In [14], the camera motion and tissue deformation are simultaneously estimated based on a respiratory model of the tissue motion. Recently, Zhang et al. [15] propose a novel system for autonomous ultrasound scanning under tissue motion. While in [16], a tissue deformation recovery method was implemented based on a probabilistic tracking and surface mapping. Because it is possible to realize from all these works, the intra-operative US-scanning procedure had many different critical aspects that have been addressed into research.

C. Contribution

Our paper presents a new framework designed for the automated localization of a pneumatically attachable flexible rail. The design of this new system has been presented in a separate paper named Pneumatically Attachable Flexible Rails for Track-Guided Ultrasound Scanning in Robot-Assisted Partial Nephrectomy A Preliminary Design Study* that has been attached to this submission as multimedia material in .pdf and that is also under consideration as a joint submission for RA-L and ICRA 2019. This will enable swift, effortless and accurate track-guided US-scanning of kidney surface, Fig.1. This system has never been used before, neither in physical studies or clinical practices.

More specifically, we propose a platform architecture along with a customized algorithm which presents: a calibrate system environment with an initial comparison of two surface registration techniques. The work done in [9] has been now applied to a real pig kidney. An imaging technique for the system detection and a pre-operative trajectory planning supported by a control scheme based on visual feedback to monitor the surgical tool. In the overall framework, the surgeons are considered part of the loop as they have to interact with the task execution and as a supervisor in case of critical conditions.

A first clinical study has been held with a pool of four surgeons trying for the first time the system in a OR-type of environment. Results obtained from the surgical acquisitions have been compared with the automatic execution of the same task. Interesting considerations were gathered also in term of improvement in the system design.

The remainder of the paper is organized as follows: in section II we present a general overview of the newly designed system and the experiment environment. Section III contains the main methodologies describe as: description of system calibration in *A*. Rail detection algorithm and surface acquisition for kidney registration in *B*, followed by spatial trajectory planning and control feature in *C*. *D* concludes the section with surgeon data acquisition description. The results of the system performances are shown in section IV and the paper concludes with a discussion of findings and some planned future work.

II. System Overview

Platform configuration - The robotic system employed to conduct our automations experiments is the first generation da Vinci robot equipped with the dVRK platform. The first da Vinci Patient Side Manipulator (PSM1) is equipped with the Large Needle Driver (LND), while the PSM2 holds the Pro-Grasp tool, Fig.2. Fig.2 also shows the new rail device that can potentially be used to guide imaging probes.

The black rail prototype in Fig.2 is attached on the kidney surface with the use of a series of bio-inspired vacuum suckers and it is used as a guide on which the surgeon attaches and slides the drop-in US probe. The design and mechanism of the vacuum pressured suckers is based on the fabrication octopus suckers. A 3D printed model of the drop-in US-probe (Hitachi-Aloka) is shown in white polymer with the customized connector already assembled onto it. Everything has been designed in order to be compatible with an auxiliary trocar port used in surgical practice. The drop-in US-probe is moved along the rail to perform a virtual scan, outlining the tumour and hence, the margin of resection. Despite the possibility of many different design configurations, for this

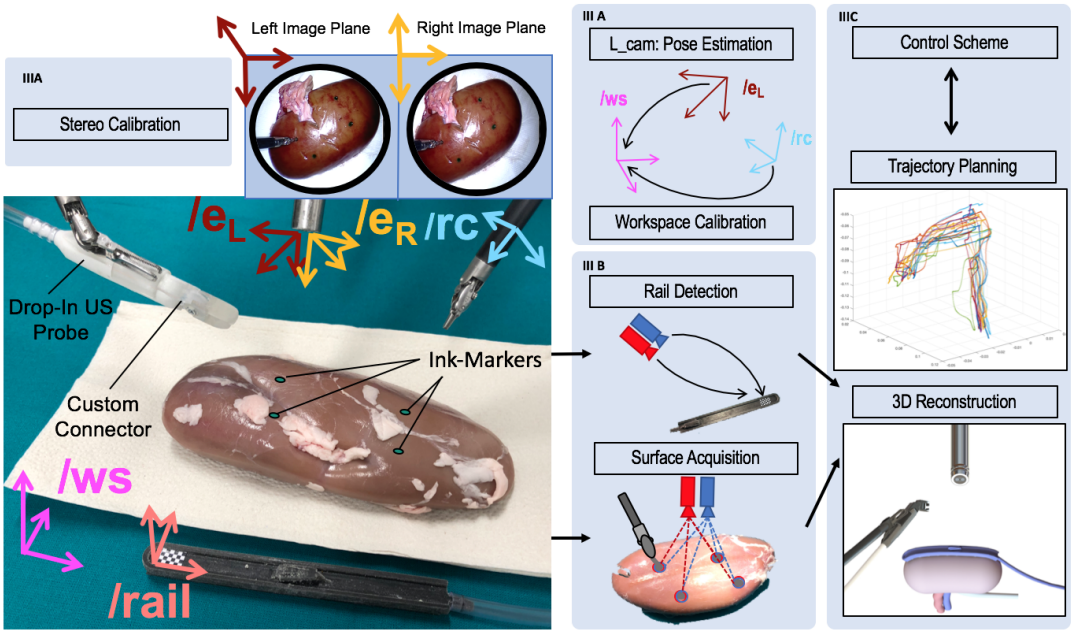

Fig. 2: Representation of the system pipeline from the platform and the methodology point of view. On the bottom left part is shown ex-vivo pig kidney, with the two robotic tools, the stereo endoscope, the black sucker rail, and the drop-in US probe. The 3D printed probe is already assembled with a customized connector for enabling the slide. Four ink markers used for surface registration are highlighted on the kidney surface. The notation "/" is used to define orthogonal clockwise reference frame systems. On the top left of the figure, there is the view coming from the left and right camera. On the right side, the ROS-node architecture is summarised according to the different methodologies described in the labeled sections.

work we used a square and continuous patterned suckers due to the higher attachment force it is able to achieve.

Software configuration - A custom ROS architecture was developed embedding the different software algorithms, right part Fig.2. To enhance the accuracy of the system we applied a well-known robotic calibration process shown in (IIIA) [17]. The dVRK console displays the surgical scene thanks using the stereo laparoscope cameras and the MATLAB stereo camera calibration toolbox [18] was used, using as input 45 image pairs of a 7 row by 10 column checkerboard all from different ECM poses.

Robot calibration involves making minor adjustments to kinematic model parameters to account for factors like manufacturing tolerances and other sources of error to increase model accuracy. The dVRK PSMs are characterized by set-up Joints (SUJ) and active joints. It worth notice that the accuracy of the instrument tip is generally more sensitive to small angular error in the base joints than in the more distal ones. Taking into account this, we follow an approach similar to [9] attaching the base coordinate frame at the beginning of the active joints. The workspace calibration is defined by the transformation between the workspace and the remote centre of motion of the arm.

A pure vision node (IIIB) was necessary to deal with the rail tracking and the kidney surface registration. The control scheme node (IIIC) was enhanced to face users requirements and a new set of experiments were conducted to evaluate the performance and robustness of the control scheme with the surgeon in the loop and compare with experiments fully teleoperated.

Notation - Scalars are represented by plain letters, e.g. λ, vectors are indicated by bold symbols, e.g. $\mathbf{e}$, and matrices are denoted by letters in sans serif font, e.g. ${}^{rc}\mathsf{T}_{ws}$. 3D points can be represented in non-homogeneous coordinates by 3x1 vectors, e.g. $\bar{\mathbf{p}}$, as well as in homogeneous coordinates by 4x1 vectors by removing a bar on the top of a symbol, $\mathbf{p}$. Orthogonal clockwise reference frames are defined with the notation of /, e.g. */ws*. A 3D point represented in /ws is denoted by $\bar{\mathbf{p}}_{\mathbf{ws}}$, while a rigid transformation from */ws* to */rc* is represented by ${}^{rc}\mathsf{T}_{ws}$, such that $\mathbf{p_{rc}} = {}^{rc}\mathsf{T}_{ws} * \mathbf{p_{ws}}$.

III. Methodology

A. System Calibration

The transformation between the image and the robot coordinates were computed and the visual accuracy of the tooltips' position was examined through experiments. The Fiducial Localization Error (FLE) allows measuring spatial data points during image-guidance [19] and in our work it was quantified both for the stereo endoscope and for the PSMs. In the case of the two cameras, 7 more additional image pairs of the checkboard were acquired after the stereo hand-eye-calibration. To triangulate checkerboard intersections extracted from these images were point-registered to the known checkboard dimensions [20]. The FLE components are determined by taking the difference in term of cartesian position between the localized points and the known checkerboard dimension following the co-registration.

For the two PSMs, equipped respectively with the LND and the Pro-Grasp, we characterized the FLE carefully prob-

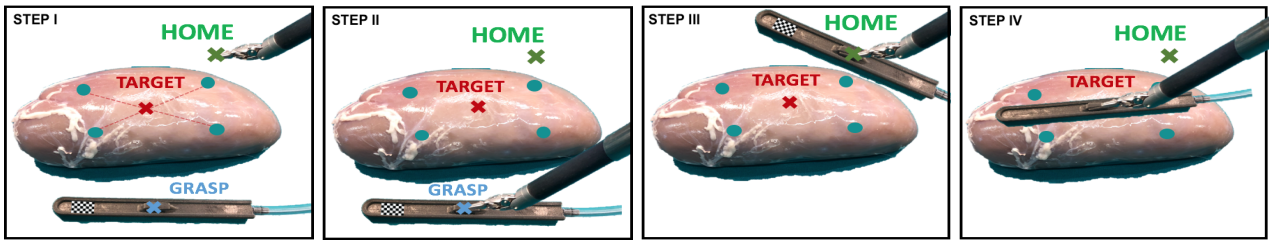

(a)

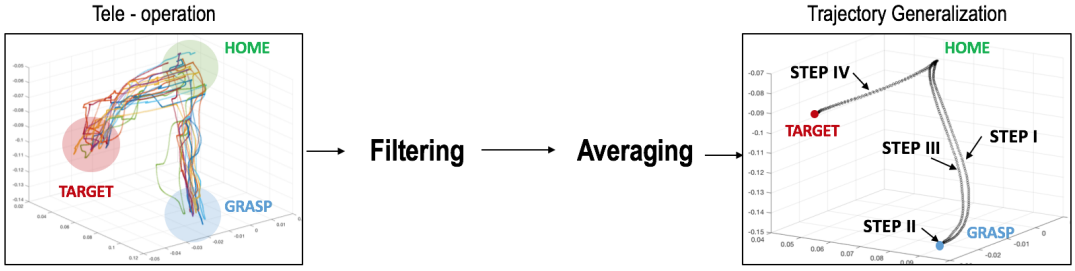

(b)

Fig. 3: Cartesian trajectory generation. (a) Representation of the different steps through which the trajectory is implemented: approaching phase where the tool moves forward the rail followed by the effective grasping phase. During the third step, the tool moves in the home position before starting the kidney targeting. (b) Blocks representation of trajectory generation steps. 10 different repetitions of the task are recorded in terms of cartesian position and joint values in tele-operation mode. Those values are then filtered and averaged in order to have a single smooth trajectory in the Cartesian space, shown by the black dotted line.

ing 20 intersection points in a 3D printed checkerboard (side length 10 mm) for each of the tools. Every time a point in the grid was touched, the robot's encoder values were recorded and used in out forward kinematic model to localize the 3D Cartesian position. The points were then registered with the known checkerboard dimensions for each PSMs.

B. Rail Detection and Surface Acquisition for Kidney Registrations

The suction rail is equipped with a small 1mm checkerboard as a fidual used to estimate pose. The pattern could easily be replaced with KeyDot®(Key Surgical, MN) [21] markers to be clinically compatible with sterilization processes. The checkerboard tracking and the stereo triangulation function from the same calibration toolbox were used to determine the location of the rail inside the workspace. This procedure includes locating the checkerboard corners with Harris corner detector using the known geometry of the checkerboard to accurately determine its pose. Knowing the model of the rail, it is then immediately possible to geometrically compute the location of the grasping site using PnP pose estimation and forward driving the trajectory of the kinematics to grasp. Registration of the soft tissue on the kidney surface for image-guidance is important since the kidney surface represents the target point for locating the image guidance rail. We extend previous methodology because in our case since a real kidney is used for the experimental setup with two methods compared in experiments [9]. The results coming from each method are compared in terms of distances between the real makers representing the ground truth.

The two methods analyzed were compared as expressed in the algorithm formulation.

Algorithm 1 Kidney Registration

ink-surgical markers definition: 4 markers with a known distance.
procedure PSM-PROBING ▷ [7]
  while $m <$ *markers* **do** ▷ For all the markers
    Localise tool tip on the m-marker
    Acquire q joints values ▷ API [22]
    r = DK(q) ▷ Foreward kinematic computation
  end while
  return r ▷ The probed cartesian position
end procedure
procedure ECM INK-MARKERS
  Color thresholding stereo pairs in HSV color space
  k-means clustering
  c - Triangulation(centroids)
  return c
end procedure

In case of the PSM-probing technique, the Cartesian position in the */rc* is computed and store in homogeneous coordinate in the matrix r. Those points are then registered in the */ws* through the following:

$$\mathsf{r}_{\mathsf{rc}} = [\mathbf{r_1}|\mathbf{r_2}|\mathbf{r_3}|\mathbf{r_4}] \tag{1}$$

$$\mathsf{r}_{\mathsf{ws}} = {}^{\mathsf{ws}}\mathsf{T}_{\mathsf{rc}} * \mathsf{r}_{\mathsf{rc}} \tag{2}$$

where ${}^{\mathsf{ws}}\mathsf{T}_{\mathsf{rc}}$ is the transformation matrix between the remote centre of the robot and the workspace, r_{rc} is the matrix of

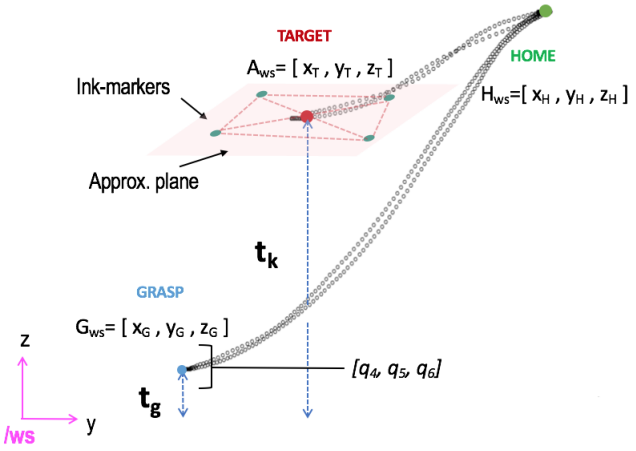

Fig. 4: closer overview of the trajectory planning step in the z-y plane. The black dotted trajectory represents the result after filtering and averaging process.

centroids mapped in the */rc*. For the detection of the ink-markers, once the centroids are clustered in each cameras reference frame, they are triangulated and reconstructed in the 3D space in order to be registered in the */ws*:

$$^{eL}X_{cL} = [\mathbf{c_{1L}}|\mathbf{c_{2L}}|\mathbf{c_{3L}}|\mathbf{c_{4L}}] \quad (3)$$

$$^{eR}X_{cR} = [\mathbf{c_{1R}}|\mathbf{c_{2R}}|\mathbf{c_{3R}}|\mathbf{c_{4R}}] \quad (4)$$

$$^{eL}X_{c} = [\mathbf{c_1}|\mathbf{c_2}|\mathbf{c_3}|\mathbf{c_2}] \quad (5)$$

$$^{rc}X_{c} = {}^{ws}T_{eL} * {}^{eL}X_{c} \quad (6)$$

Where $^{eL}X_{cL}$ represents the matrix with all the centroids detected in the left camera and $^{eR}X_{cR}$ the one detected in the right camera. $^{eL}X_{c}$ represents the matrix with the centroids reconstruct in the 3D space in respect of the left camera reference frame system. $^{rc}X_{c}$ is the matrix of centroids mapped in the */rc*.

The results coming from each method are compared in terms of distances between the real makers in the */ws* representing the ground truth.

C. Spatial trajectory planning and control features

To automatically locate the system in the target point with the robotic tool, the procedure involves two main components: generate a trajectory to ergonomically locate the rail and develop a control strategy to optimize the operational performance.

In order to position the rail on the kidney four main stages were designed in our method. First, Fig.3(a)-STEP I, the tooltip starts from a "home" position defined in the 3D space by $[x_H, y_H, z_H]$. In the second stage as shown in Fig.3(a) - STEP II, the robotic tools approaches the grasping site in the central part of the rail. $[x_G, y_G, z_G]$ is the Cartesian position of the grasping point coming from the rail detection through the stereo-camera and successively triangulate in the 3D space.

$$\mathbf{G_{eL}} = [G_x, G_y, G_z, 1] \quad (7)$$

$$\mathbf{G_{ws}} = {}^{ws}T_{eL} * G_{eL} \quad (8)$$

where

$$\mathbf{G_{ws}} = [x_G, y_G, z_G, 1] \quad (9)$$

and $\mathbf{G_{eL}}$ represents the vector with the triangulated point in the */eL*.

Then the tip moves back to the predefined home position, as sketched in STEP III. Finally, as shown in STEP IV, the tool holding the rail moves towards the kidney surface to reach the target point $[x_T, y_T, z_T]$. Fig. 4 shows how the target point is computed as the centroid of the bounding box defined by the four ink-markers. It is possible to apply this method since the curvature of the kidney surface is really small and it can be ignored.

The cartesian position of the tooltip during the transition between those declared points was computed as follows: 10 different repetitions of the same locating task were executed in tele-operation by a trained operator. During those procedures both the Cartesian and the joints values were acquired through the Intuitive Surgical Application Programming Interface (API), Fig.3(b) - left image. Those values are then filtered and averaging in order to be able to define a more precise, clear and smooth cartesian trajectory. This function is then parametrized in order to be adapted to the different values of grasping position since the rail starting position has been randomized during experimental acquisitions.

During the approaching phase in STEP II, there is the additional need to control the orientation of the tool tip in order to guarantee a solid grasp. The orientation of the tip depends on the last three active joints of the PSM arm, $[q_4, q_5, q_6]$. Those values have been obtained with the same protocol applied in case of the Cartesian trajectory. After the filter and the average step, they are used as control input for the approaching phase, Fig.4.

In order to complete the entire task, the tool tip is required to follow the pre-planned trajectory. To account for uncertainties and minor errors, some other control features were added to enhance the performance of driving the tool. Starting from the estimation of the grasping point: $\mathbf{G_{ws}}$ defines the position of the first active motion (STEP II). This point, as shown in (7), is reconstructed in the 3D space starting from the stereo pairs. Unlikely, in the da Vinci system the baseline between the two cameras is only 5.4 millimeters and this reflects consistent uncertainty in the depth estimation. Hence as a safety control, once the position of z_G is estimated, it is compared to the position of the kidney along with the same axis z_K in order to be sure that $\mathbf{t_g} < \mathbf{t_k}$ (Fig.4).

Furthermore, a controller with visual feedback was added to the robotic system to enhance the performance of driving the tool, starting from STEP II. Albeit, the system does not present any tool tracking node, once the relationship between

the rail and the tool is geometrically established by the grasping phase, it is possible to compute the same information. The position of the tool tip is extracted dynamically and transpose in the */ws* and compare to the position acquired through the dVRK and transpose in the same space.

$$e_i = ||\mathbf{p}(\mathbf{G_{eL}}(\mathbf{i}), {}^{ws}\mathsf{T}_{eL}) - \mathbf{p}_i^*|| \tag{10}$$

where i represents the time at which each frame is acquired, $\mathbf{p}_i^*$ is the current position of the tool tip in the workspace reference frame system . While $\mathbf{p}(\mathbf{G_{eL}}(\mathbf{i}), {}^{ws}\mathsf{T}_{eL})$ is the position computed from the stereo tracking of the reail held by the LNG. This error function is then minimize proceeding to the next step.

In the final STEP IV, an additional control is added in order to be sure that at the end of the task the sucker rail will be located parallel to the kidney surface. This control has been implemented with a visual feedback, knowing the rail position and the registered kidney surface, Approx. plane in fig.4. The value of the fifth joint q_5, responsible for the pitch of the tip, is consequentially modified until the distance between the rail and the kidney plane becomes null.

D. Surgeon data acquisitions

Beside the studies related to the automation of the taks, a clinical study has been held as first validation and term of comparison. Four surgeons took part to the acquisitions, with different years of experience in robotic surgery all specifically focused on urology. Since surgeons were never got in tough with the system in order not to influence their action no instructions were given at the beginning and there was no possibility of information exchange between them until the end of all the acquisitions.

As a starting step a briefly introduction of the system was given to all of them just in purely descriptive terms. The acquisitions were organised as follows: they have to complete three main tasks "location", "sliding", and "kidney motion". Each task has been repeated three times in order to quantify the improving rate. For each task in each execution the variables measured were: execution time $\mathbf{T_{exe}}$, success rate **SR**, difficulty in using the system **DF** scored from 1 to 10, and how much they were willing to use the system in real clinical practice **WU** scored from 1 to 10.

IV. Experiments and Results

A. Calibration and Surface Registration Accuracy

Calibration - The FLE components for the stereo endoscope were taken as a difference between the localized points and the known checkerboard dimensions following co-registration. For the two PSMs arms equipped with LND and pro-Grasp the component of the FLE were taken as the registration error of the point-sets as before for the ECM. A Quantile-Quantile (QQ) plot was used to characterize the FLE distribution. The mean and the standard deviation of the FLE magnitudes are shown in Table I.

As it is possible to see in the table, the value related to the PSM2 equipped with the Pro-Grasp are significantly higher than the one with the LND. During the probing procedure, we used the nominal DH parameters provided with the Intuitive Surgical API for both the robotic tools. In the case of the Pro-Grasp, the probing procedure results being really inaccurate due to the hardware design. With the LND the last four joints configurations allow a precise and accurate localization of the tool tip during the acquisition procedure, while in case of the pro-grasp the rounded tip brings to the resulting inaccuracies.

TABLE I: FLE for each da Vinci manipulators. The value are expressed in mm

	Mean and s.d.
PSM1	1.10 ± 0.58
PSM2	3.33 ± 0.78
ECM	0.93 ± 0.56

As an outcome of those results, we decide to use the LND as grasping tool during the experimental acquisition instead of the Pro-Grasp, despite the rail has been designed for that particular tool.

Kidney Registration - The accuracy of the registration applied is quantified by the error in the markers recontruction for each methods in terms of Euclidean distance between the markers themselves, TABLE II.

TABLE II: Error measured in terms of Euclidean Distance between the ink-markers. The values are expressed in mm.

Ground Trouth Distance	**Surface tracing with PSM Intrument Tip**	**ECM Triangulation of Surgical ink Markers**
50	51.23 ± 0.44	54.10 ± 0.88

Unsurprisingly, given the small intraocular distance of 5.4 mm between the stereo camera in the da Vinci endoscope, localization registration with PSMs was more accurate than with endoscope-based technique.

B. Results from Task Automation

As a preliminary test, we focus on the repeatability of the task in order to be sure the kinematic can be used for guiding the da Vinci. 6 different acquisition were recorded of the same task with the same initial condition. The rail is positioned in the field of view of the endoscope and the LND tooltip starts from the "home" position. The task is considered completed once the tool has grasped the rail and after precisely locate in on the kidney surface it goes back to the "home" position.

Despite the starting position of the rail was always the same, due to errors coming mainly from the triangulation, the Cartesian position of the grasping point slightly vary among the 6 repetitions. The boxplots in Fig. 5 show the mean value according to the three Cartesian axes in the */ws* of the position estimated during the acquisitions. As it is possible to notice the value related to the z-ax or depth estimation are greater than the other two axes, confirming that the main error component is due to depth estimation.

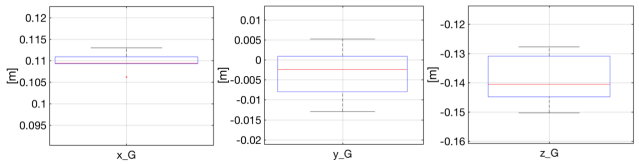

Fig. 5: Repetability test: the boxplots show according to the three different axes the mean value of the grasping point estimate in the 3D space for all the six acquisitions.

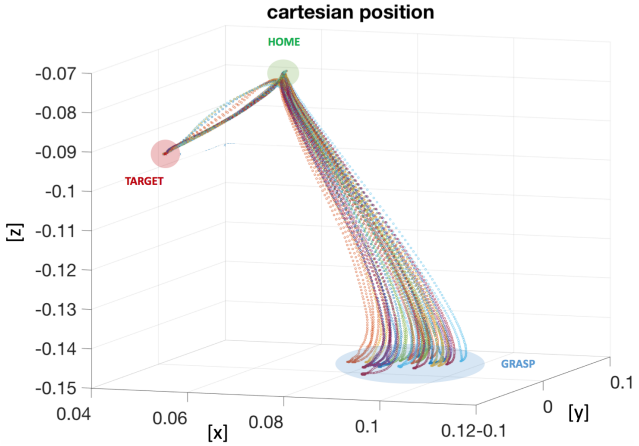

Fig. 6: Representation of the Cartesian position of the tooltip in the workspace in m. 30 out of 40 acquisitions are represented. All successful and all starting with a different initial position of the rail.

Those values are still small enough to guarantee a correct grasp in all the repetitions.

A dataset of 40 acquisitions has been recorded to test the overall architecture. The experiment was defined as follows: the rail was randomly inserted inside the field of view of the stereo-endoscope in order to emulate the surgical environment where the system would be inserted through the support trocar. If the rail reached an upside-down position it was relocated by the assistant using the suction pipe. Once the system is detected inside the endoscope field of view the robot starts its motion grasping the target and locating it on the organ surface following the pre-planned trajectory. The task in consider concluded once the rail is effectively in suction with the kidney itself. As shown in Fig. 6, the experiment has a success rate of 35 acquisitions over 40, while in the remaining 5/40 the tooltip was not able to reach the rail (Fig.7). Additionally, as it is highlighted from the yellow circle in the Fig.7, in 4/40 acquisition the task was correctly completed but estimating the rail position lower than the rail position, generating a small slide of the rail before the effective grasp, showed bu the horizontal dotted line. The average time among all the acquisitions was 42 seconds.

C. Surgeons acquisitions

Four surgeons took part in the experimental study and Table III reports all the results from the different experimental

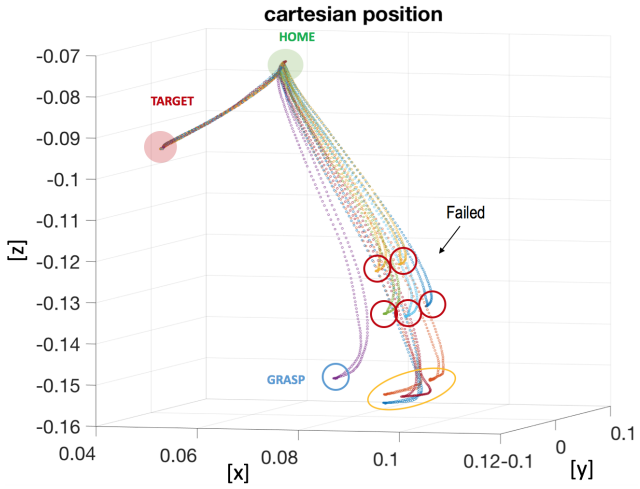

Fig. 7: Representation of the Cartesian position of the tooltip in the workspace in m. 10 out of 40 acquisitions are represented. The blue circled one represents a well-executed task plot as a visual reference for the other trajectory. The red circles indicate the 5/40 executions failed, while in the yellow ones the task was properly executed but with a not precise depth estimation.

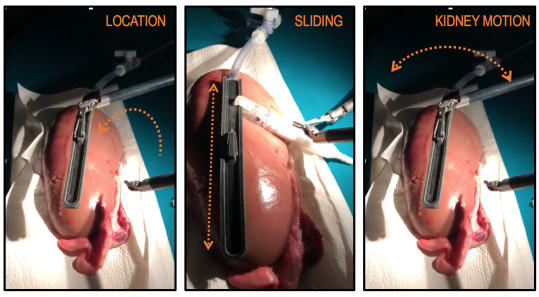

Fig. 8: Representation of the three experimental tasks executed by the surgeons.

acquisitions. Values are shown as the mean values among the three different repetitions of the same task. The different surgeons are represented by "**S**" followed by the number. They were all surgeons with experience in robotic surgical operation with the da Vinci. The three tasks they had to complete are described as follow: **Location** is represented by the same task that has been automatized. The surgeon has to grasp the rail and locate it over the kidney surface in order to guarantee a correct suction. The **Sliding** task starts right after: once the rail is in place the surgeon has to precisely locate the probe adaptor on the rail and complete a full slide back and forth, concluding the task removing the probe from the rail. The last task, **Kidney motion**, the rail is grasped while in suction with the kidney surface and used to move the kidney with circular movement in respect to the main longitudinal axis as can be visualised in Fig.8.

The execution time T_{exe} is measured in minutes. The Success Rate (SR) represents after how many attempts they actually manage to complete the task. The difficulty level using the system (DF) is a subjective value scored by each surgeon between 1 and 10. While the last value (WU) is

scored exactly like the previous one but it represents the willingness of using the system in actual clinical practice.

TABLE III: The values in the table represent the average values among the three repetitions for each task. y.o.e stays for "years of experience" in robotic surgical operation. The execution time is reported in minutes.

	Surgeons Informations	LOCATION				SLIDING				KIDNEY MOTION			
		T_{exe}	SR	DF	WU	T_{exe}	SR	DF	WU	T_{exe}	SR	DF	WU
S1	Urology 4 y.o.e.	1	1/1	1	1	5	1/6	7	0	1	1/1	1	8
S2	Urology 1 y.o.e.	1.5	1/5	3	0	6.3	1/7	6	0	1.2	1/2	2	4
S3	Urology 3 y.o.e.	3	1/3	5	5	8	1/8	8	5	1.4	1/2	2	8
S4	Urology 2 y.o.e.	2.5	1/4	4	4	7.1	1/5	7	4	1.1	1/1	3	7

V. Conclusion and Future work

The preliminary experiments presented in this paper show that the automatic localization of the newly designed imaging rail system is realisable. The architecture we presented can be computationally executed for locating the probe and moving the robotic instruments based on a calibrated system and a pre-planned trajectory.

New results have been presented for registering the surface of a porcine kidney to the robotic coordinate frame extending previous work [9]. The calibration process allowed a comparison between the accuracy of the two robotic tools, LND and Pro-Grasp, based on which the experimental set up has been built in order to have the level of accuracy required with the LND was used primarily. Using additional control features increased the stability of the executed automation grasping.

From a clinical point-of-view, our case study presents experiments where surgeons tried for the first time both the new rail system design and also the automation procedure. The experiments highlighted the need to build inherent user flexibility and make the system compatible with every tool, not only the LND and Pro-Grasp, to reflect the same outcome of the robotic calibration. This might affect a new re-design process for the rail in terms of handles and ergonomic features. In terms of execution time, as it is possible to notice in the results, the robot is able to execute slightly faster the task of placement which seems to be a promising albeit preliminary result.

Several difficult challenges remain. One is increasing and incorporating mitigation strategies for the variables coming from a real clinical environment, taking into account kidney motion and deformation and a highly vascularized environment where bleeding can cause occlusion and vision system failure. This has potentially adverse effects on the surface registration process. As future step, we will work on actually automatize all the three tasks that have been executed by the surgeons in order to have a more complete comparison. With regards to further ways of validating the system, a real US-probe will be used in order to compare the outcome of the two scanning procedure, automatic and teleoperated one, in terms of tumor localization accuracy.

References

[1] I. Surgical. Frequent asked questions. [Online]. Available: http://www.davincisurgery.com/da-vinci-gynecology/da-vinci-surgery/frequently-asked-questions.php

[2] H. J. Marcus, A. Hughes-Hallett, C. J. Payne, T. P. Cundy, D. Nandi, G.-Z. Yang, and A. Darzi, "Trends in the diffusion of robotic surgery: A retrospective observational study," *MICCAI*, vol. 13, no. 4.

[3] S. Kaul, R. Laungani, R. Sarle, H. Stricker, J. Peabody, R. Littleton, and M. Menon, "Da vinci-assisted robotic partial nephrectomy: Technique and results at a mean of 15 months of follow-up," *European Urology*, vol. 51, no. 1, pp. 186 – 192, 2007.

[4] C. G. Rogers, A. Singh, A. M. Blatt, W. M. Linehan, and P. A. Pinto, "Robotic partial nephrectomy for complex renal tumors: Surgical technique," *European Urology*, vol. 53, no. 3, pp. 514 – 523, 2008.

[5] S. B. Bhayani, "da vinci robotic partial nephrectomy for renal cell carcinoma: an atlas of the four-arm technique," *Journal of Robotic Surgery*, vol. 1, no. 4, pp. 279 – 285, 2008.

[6] S. D. Herrell, D. M. Kwartowitz, P. M. Milhoua, and R. L. Galloway, "Toward image guided robotic surgery: System validation," *The Journal of Urology*, vol. 181, no. 2, pp. 783 – 790, 2009.

[7] H. O. Altamar, R. E. Ong, C. L. Glisson, D. P. Viprakasit, M. I. Miga, S. D. Herrell, and R. L. Galloway, "Kidney deformation and intraprocedural registration: A study of elements of image-guided kidney surgery," *Journal of Endourology*, vol. 25, no. 3, pp. 511–517, 2011.

[8] A. B. Benincasa, L. W. Clements, S. D. Herrell, and R. L. Galloway, "Feasibility study for image-guided kidney surgery: Assessment of required intraoperative surface for accurate physical to image space registrations," *Medical Physics*, vol. 35, no. 9, pp. 4251–4261, 2008.

[9] A. R. M. S. S. D. S. D. H. R. J. W. James M. Ferguson, Leon Y. Cai, "Toward image-guided partial nephrectomy with the da vinci robot: exploring surface acquisition methods for intraoperative re-registration," pp. 10 576 – 10 576 – 11, 2018.

[10] C. Schneider, J. Guerrero, C. Nguan, R. Rohling, and S. Salcudean, "Intra-operative "pick-up" ultrasound for robot assisted surgery with vessel extraction and registration: A feasibility study," in *MICCAI*, R. H. Taylor and G.-Z. Yang, Eds. Springer Berlin Heidelberg, 2011, pp. 122–132.

[11] O. Mohareri, J. Ischia, P. C. Black, C. Schneider, J. Lobo, L. Goldenberg, and S. E. Salcudean, "Intraoperative registered transrectal ultrasound guidance for robot-assisted laparoscopic radical prostatectomy," *The Journal of Urolog*, vol. 193, no. 1, pp. 302 – 312, 2015.

[12] C. Vienne and A. Krupa, "Intensity-based ultrasound visual servoing: Modeling and validation with 2-d and 3-d probes," vol. 29, pp. 1003–1015, 08 2013.

[13] P. Pratt, A. Hughes-Hallett, L. Zhang, N. Patel, E. Mayer, A. Darzi, e. N. Yang, Guang-Zhong", J. Hornegger, W. M. Wells, and A. Frangi, "Autonomous ultrasound-guided tissue dissection," in *MICCAI 2015*, 2015, pp. 249–257.

[14] P. Mountney, e. T. Yang, Guang-Zhong", N. Navab, J. P. W. Pluim, and M. A. Viergever, "Motion compensated slam for image guided surgery," in *MICCAI 2010*, 2010, pp. 496–504.

[15] L. Zhang, M. Ye, P. Giataganas, M. Hughes, and G. Yang, "Autonomous scanning for endomicroscopic mosaicing and 3d fusion," *CoRR*, 2016.

[16] S. Giannarou, M. Ye, G. Gras, K. Leibrandt, H. J. Marcus, and G.-Z. Yang, "Vision-based deformation recovery for intraoperative force estimation of tooltissue interaction for neurosurgery," in *Internat. Journal of Computer As. Radiology and Surgery*, 2016.

[17] W. Khalil and E. Dombre, *Mod., Ident. and Control of Robots*, 3rd ed. Bristol, PA, USA: Taylor & Francis, Inc., 2002.

[18] Z. Zhang, "A flexible new technique for camera calibration," *IEEE Trans. on Pattern Anal. and Machine Intelligence*, vol. 22, no. 11, pp. 1330–1334, 2000.

[19] J. M. Fitzpatrick, J. B. West, and C. R. Maurer, "Predicting error in rigid-body point-based registration," *IEEE Transactions on Medical Imaging*, vol. 17, pp. 694–702, 1998.

[20] C. D'Ettorre, G. Dwyer, X. Du, F. Chadebecq, F. Vasconcelos, E. D. Momi, and D. Stoyanov, "Automated pick-up of suturing needles for robotic surgical assistance," *CoRR*, vol. abs/1804.03141, 2018.

[21] P. Pratt, C. Bergeles, A. Darzi, e. P. Yang, Guang-Zhong", N. Hata, C. Barillot, J. Hornegger, and R. Howe, "Practical intraoperative stereo camera calibration," in *MICCAI 2014*. Springer International Publishing, 2014.

[22] P. Kazanzides, Z. Chen, A. Deguet, G. S. Fischer, R. H. Taylor, and S. P. DiMaio, "An open-source research kit for the da vinci surgical system," in *IEEE Intl. Conf. on Robotics and Auto. (ICRA)*, Hong Kong, China, 2014, pp. 6434–6439.